System architecture and business opportunities for Applied-Field Magnetoplasmadynamic Thrusters

IEPC-2019-801

Presented at the 36th International Electric Propulsion Conference
University of Vienna • Vienna, Austria
September 15-20, 2019

Marcus Collier-Wright[1], Bartomeu Massuti Ballester[2], Manuel La Rosa Betancourt[3], Maieul Girard[4], Ryan O'Regan[5]
Pi Integral Solutions, Köln, 50674, Germany

Georg Herdrich[6]
University of Stuttgart, Institute of Space Systems, Stuttgart, 70569, Germany

Julien Tanchon[7], Jerome Lacapere[8]
Absolut System SAS, Grenoble, 38170, France

and

Markus Bauer[9]
THEVA Dünnschichttechnik GmbH 2, Ismaning, 85737, Germany

Abstract: To date orbital transfers of large spacecraft and high ΔV missions from Low Earth Orbit (LEO) to Geostationary Earth Orbit (GEO), lunar transfer, or interplanetary trajectories are still mainly conducted using chemical propulsion systems. In order to overcome limitations in ΔV and the high launch propellant mass imposed by these systems, efforts to develop and mature single-engine Electric Propulsion (EP) technology of 20 and 100kW, with the ability to scale to over a MW, are already ongoing. This paper evaluates the current developments of steady-state Applied-field Magnetoplasmadynamic Thruster (AF-MPDT) technology, which is currently experiencing a renaissance as the growing interest in lunar and Mars missions, as well as orbital traffic, is reviving the market for high-power propulsion systems. Moreover, the application of high-temperature superconductors (HTS) and the commercial maturity achieved in the production of HTS tapes and coils open a new field of possibilities for AF-MPDT. Second generation HTS enable EP based on HTS coils capable of producing high magnetic fluxes, which allows for an extended operation range for AF-MPDT with higher discharge voltage, leading to lower arc currents and the application of LaB6 hollow cathodes. After an initial overview of the current developments in AF-MPDT and HTS technologies, the system architecture of an AF-MPDT using HTS coils is introduced. This is followed by a market analysis and an evaluation of the capabilities for AF-MPDT in

[1] Project Manager Electric Propulsion, marcus.collier-wright@pintegralsolutions.de
[2] Consultant Electric Propulsion, bartomeu.massuti@pintegralsolutions.de
[3] Founder & Director, manuel.la-rosa@pintegralsolutions.de
[4] Project Support, maieul.girard@pintegralsolutions.de
[5] Project Support, ryan.o-regan@pintegralsolutions.de
[6] Head of Department, Plasma Wind Tunnels and Electric Space Propulsion, herdrich@irs.uni-stuttgart.de
[7] R&D Manager, julien.tanchon@absolut-system.com
[8] Scientific Director, jerome.lacapere@absolut-system.com
[9] VP Business Development, bauer@theva.com

three different mission scenarios, which are (1) space tugs for orbit raising of GEO satellites; (2) cargo and logistics transfers for lunar and cis-lunar missions; (3) unmanned interplanetary transfers for human exploration to near earth objects and Mars. The paper evaluates the system requirements and the benefits of using AF-MPDT compared to other electric propulsion systems for the mission scenarios.

Nomenclature

B	=	Magnetic Field Strength
j	=	Discharge Current
I_{sp}	=	Specific Impulse
m_{cargo}	=	Cargo Vehicle Mass
m_{eps}	=	Electric Propulsion System Mass
m_{prop}	=	Propellant Mass
m_{tv}	=	Transfer Vehicle Mass
P_{in}	=	Input Power
P_{tot}	=	Total Mission Power
α	=	Thrust Density
η	=	Thrust Efficiency
γ_t	=	Thruster Specific Weight
γ_p	=	PPU Specific Weight
ΔV_{out}	=	Outbound Delta-V
ΔV_{in}	=	Inbound Delta-V

I. Introduction

The next revolution in space will be driven by high-power electric propulsion (EP) technology. Replacing cost-heavy and inefficient chemical propulsion with electric propulsion systems (EPS) will launch the development of the space market into new heights. This will disrupt the high power space market as numerous missions, from space tugging to moon- and deep-space architectures, become ever more technologically and economically viable. However, the necessary cost- and propellant-efficient EPS operating at increasing high-power classes are not yet available.

The current commercial EP technologies feature thrusters of power classes up to around 10kW, with clustering used for high-power missions up to 40kW[1]. Although this clustering has a positive effect on the system redundancy, issues related to thermal management, power losses, mass margins and complexity limit the number of thruster units per system towards higher powers. Thus, single high-power units are needed. Furthermore, the objectives in the 2015 NASA roadmap[2] clearly indicate the need for maturation of single-engine technology of around 100kW with the ability to scale to over a MW. In this regard, the X3 100kW class nested-channel Hall Effect Thruster (HET) is currently under development[3]. When assessing the most suitable EP technology, scalability to high-powers is of vital consideration and is different for each existing EP technology. While Gridded Ion Thrusters (GIT), HET and Highly Efficient Multistage Plasma Thrusters (HEMPT) are currently at a high Technology Readiness Level (TRL), these systems are most suitable for low- and medium-power level operation, with significant challenges concerning upscaling to higher powers.[4]

The Applied-Field Magnetoplasmadynamic Thruster (AF-MPDT) is one of the most promising technologies for providing the necessary performance for the next phase of space logistics and in-space infrastructure applications. AF-MPDT, due to its robustness and simplicity, is inherently well suited for high-power regimes and provides the highest thrust-per-unit surface of plume section compared to any other EP technology. AF-MPDTs have been researched since the early 1960s with a variety of designs, operating regimes and optimisation approaches. Thrusters operating at powers between 2kW and 4MW and applied magnetic field strengths up to 0.6 T have been investigated[5]. Research has primarily involved the use of Argon, Hydrogen and Lithium propellants, but significant amounts of data also exist for ammonia, nitrogen, helium and caesium. Currently, the typical performance is in the 2000-6000 s Isp range at maximum efficiencies of 30-70%.[6]

MPD thruster designs can be categorised as either self-field or applied-field. In self-field designs, the magnetic field is induced by the electrical current flowing between the thruster anode and cathode. Applied-field designs, on the other hand, use dedicated external magnets to provide the magnetic field. Self-field designs require high powers and high currents to generate the required magnetic field strength for operation. This power is on the order of several hundred kW, while the high currents have an extremely adverse impact on cathode degradation and hence thruster lifetime. Hence, MPD research to date has been primarily focused on applied-field designs.

In this paper, the research history of AF-MPDTs is covered and advances in the development of HTS technology are discussed. The conceptual system architecture of an AF-MPDT incorporating HTS is then explored. Finally, the economic superiority of AF-MPDTs will be demonstrated by performing a market analysis and comparison, investigating the effects of replacing status-quo EPS with AF-MPDT technology in various high-power mission scenarios.

II. Research and development of AF-MPDT technology worldwide

There have been two periods of major activity in AF-MPDT research. In the first, from the early-1960s until the mid-1970s, the development efforts focused on reducing the power consumption of AF-MPDT (< 30kW) to meet spacecraft power restrictions. In this regard, Giannini Scientific Corporation, Electro-Optical System, AVCO Research Laboratory, and AVCO Space Systems Division, supported by tests at NASA-Langley and NASA-Lewis, led the research in the USA.[5] The development of an Ammonia-fed AF-MPDT by McDonnell Douglas Corporation, Caesium- and Lithium-fed AF-MPDT at the Los Alamos National Laboratory, and noble gas-fed AF-MPDT at the German Aerospace Centre (DLR, formerly DFVLR) followed the research.[7] The second period started in the late 1980s focusing on higher powers (> 100kW) with longer lifetimes suitable for planetary exploration and heavy-cargo Earth orbit missions. The most significant activities were conducted by Myers at NASA-Glenn[8] for the USA, the Moscow Aviation Institute (MAI[9]) in Russia and Osaka University[10] in Japan. The global development of AF-MPD technology is presented in Figure 1.

Currently, AF-MPDT technology is under development in Germany (IRS, University of Stuttgart[11]), China (Beihang University[12]), Japan (University of Nagoya[13] and Osaka University), the USA (Princeton University[14]) and Russia (MAI). All results thus far have been obtained using technology demonstrators tested in laboratory environments at TRL ≤ 4. In recent years, the Institute of Space Systems (IRS) at the University of Stuttgart has developed AF-MPDT laboratory models and optimising test facilities aimed towards high-power operation in steady-state mode. Within the HiPER project, the nominal 10kW AF-MPDT ZT1 (similar in design to the X16 from DFVLR in 1974) was successfully set into operation and, at 100mT of applied field, showed good agreement with DLR trends, demonstrating a remarkable performance of 40 % thrust efficiency at an arc power of only 12kW using argon. Most recently, and within an ESA Technology Research Programme activity, the laboratory prototype SX3 demonstrated that an AF-MPDT operating at discharge currents as low as a few hundred Amps can result in high thrust performances. With an applied magnetic field of 400 mT and operating with argon, SX3 achieved thrust efficiencies of almost 60%, >4000s I_{sp}, a maximum thrust of about 3.34 N at powers between 50 and 114kW, and discharge currents between 320 and 750A.[11]

As Figure 1 shows, a wide range of power classes have been researched. In general, the highest efficiencies have been achieved at higher powers. Notably, there has been very little research on magnetic field strengths stronger than 0.6T. This is due to the significant challenges associated with generating such fields with conventional technologies. Testing of a superconductor-based AF-MPDT will provide important data to further expand the existing AF-MPDT research database. The results of the SX3 are the most promising published experimental results of an AF-MPDT to date, and indicate that a high performance can be achieved at low discharge currents.

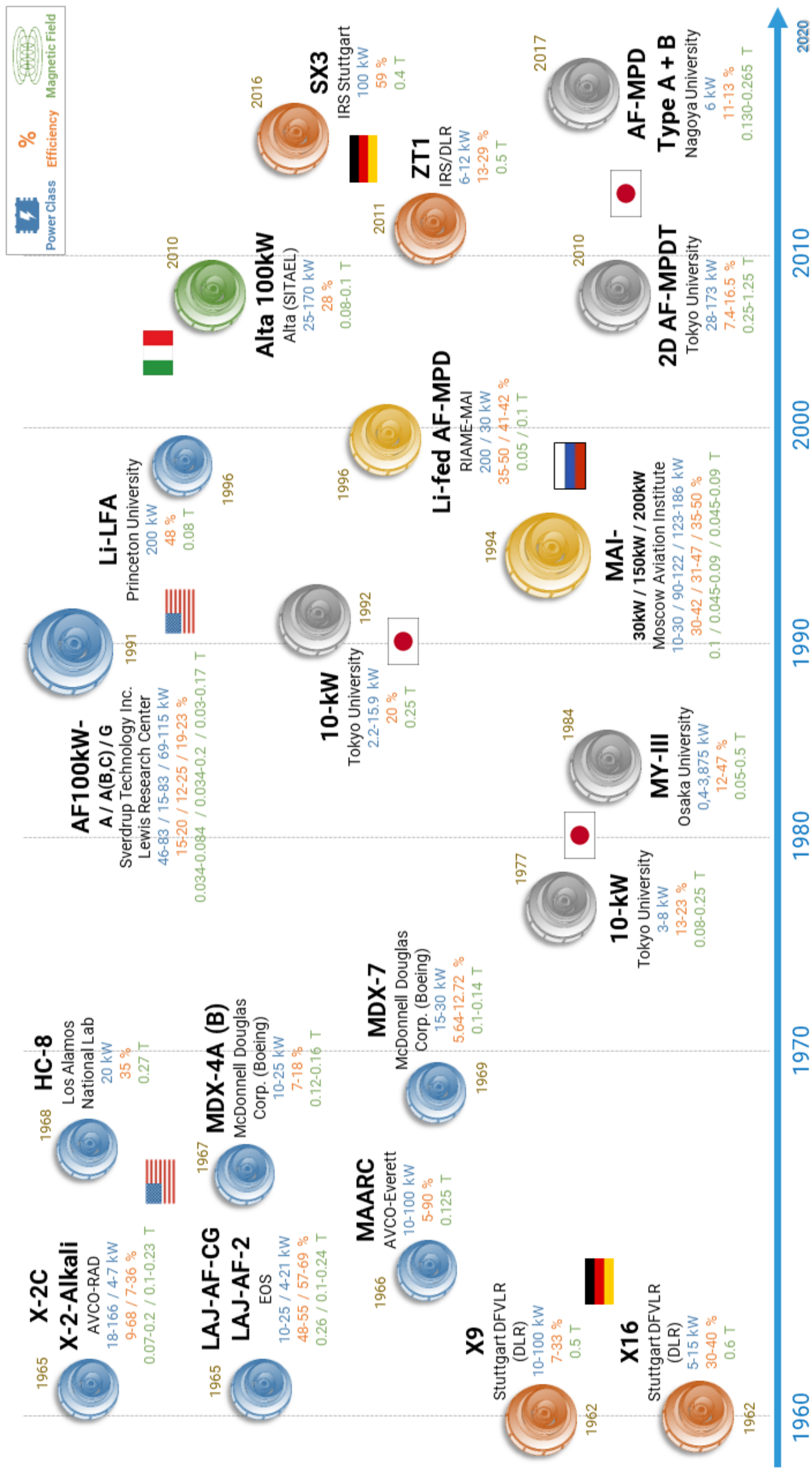

Figure 1: R&D History of AF-MPD Thrusters around the world, showing the power class of each thruster, the magnetic field strengths, and the thrust efficiency.

III. Advances in High Temperature Superconductors in the past 10 years

Superconductivity was discovered in 1911 when Dutch Physicist H. K. Onnes cooled Mercury metal to an extremely low temperature and observed that the metal exhibited zero electrical resistance. In 1986, J. G. Bednorz and K. A. Müller discovered oxide-based ceramic materials that demonstrated superconducting properties as high as 35 K. This was quickly followed in early 1997 by the announcement by C. W. Chu of the cuprate superconductor $YBa_2Cu_3O_7$ (YBCO) functioning above 77 K - the boiling point of liquid nitrogen - making them more suitable for commercialisation as they require less cryo-cooling power. Since then, extensive research worldwide has uncovered many more oxide-based superconductors with potential manufacturability benefits and critical temperatures as high as 135 K. Superconducting materials with a critical temperature above 23 K are known as High Temperature Superconductors. Since 1987, the development of so-called coated conductors (CC) - long, flexible wires with thin layers of cuprate - has been a triumph of scientific insight, sophisticated processing and determined scale-up efforts. These CCs are promising for superconducting magnet applications because of their high critical current density with a low dependency on the external magnetic field, good mechanical properties and reasonable cost, which offer opportunities to develop ultra-high-field magnets.

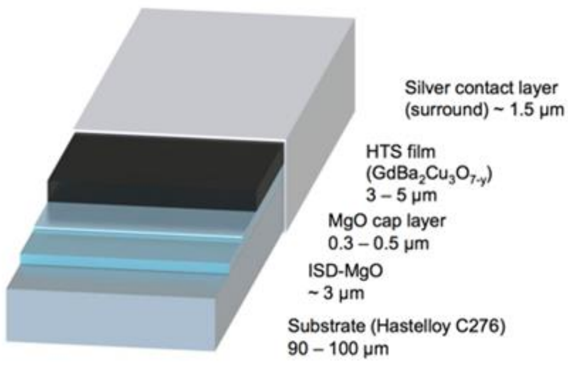

Figure 2. THEVAs CC Tape Architecture

The best-known high temperature superconductor is Yttrium-Barium-Copper oxide (YBCO), while other very similar materials are used today for industrial HTS wires as they offer improved performance. One example is Gadolinium-Barium-Copper oxide (GdBCO). These wires are produced as a multi-layer system on a 0,05 mm thin metal substrate which is a Nickel Chrome alloy. Two Magnesium Oxide buffer layers act as a diffusion barrier and provide a suitable crystalline oriented surface for the GdbCO film deposited on top. Finally, a very thin silver contact layer and a copper layer are applied. All are deposited by Electron Beam Physical Vapour Deposition, which is a well-known and scalable technology for producing thin films on an industrial scale. This technology offers advantages such as high evaporation rates, low substrate temperature, flexibility on selecting evaporation materials and a high performance due to quality consistence along the length of the tape.

This high level of maturity has led to achieving a market situation of economies of scale. The worldwide installed capacity for 2G HTS tapes is around 1,000 km/year. Critical factors for success such as high throughput, low material costs and a high yield have already been demonstrated with this production. Further increase in demand is expected so that the price of the DD will decrease due to economy of scales as well as ongoing improvements in production technology. The most prolific producer of this technology in Europe is THEVA Dünnschichttechnik, based in Bavaria, Germany. Their CC tape architecture is shown in Figure 2. With their state-of-the-art facilities, pictured in Figure 3, they have a production capacity of 120km/year of CC tape.

Figure 3. THEVAs CC production facility

Among their many uses, HTS are particularly suitable in cases where strong magnetic fields are required as a substitute for traditional copper electromagnets. This is thanks to their high current densities (typically up to 500A/mm^2 [16]), which are two orders of magnitude greater than copper wires. HTS thus enable the generation of magnetic fields using coils with a significantly reduced mass, volume and power consumption. These characteristics make them ideal for space applications such as radiation shielding and re-entry protection systems. For EP systems, which to date have only used permanent magnets, HTS coils enable the generation and tailoring of higher magnetic fields while still maintaining a low system weight and mass. Permanent magnets become significantly heavier and larger when stronger magnetic fields are required. As well as their application within

AF-MPDTs, HTS can potentially be used in self-field MPD thrusters, High Efficiency Multistage Plasma Thrusters, Helicon Plasma Thrusters, and Hall Effect Thrusters. Thus, the development of HTS-based subsystems for AF-MPDT has a high technology transfer potential to other EP technologies.

IV. System Architecture of an Applied-Field Magnetoplasmadynamic Thruster using High Temperature Superconductors

There are several traits that characterise AF-MPDT designs. Most designs are axially symmetrical, with a rod-shaped cathode located on the thruster centerline and a cylindrical anode positioned concentrically with the cathode. This configuration produces a radial discharge current with an induced azimuthal magnetic field. The applied magnetic field is produced by magnets positioned cylindrically around the anode, generating a magnetic field in the axial direction. This results in an overall helical magnetic field topology due to the combination of the axial and azimuthal fields. Downstream of the main discharge, the diverging axial magnetic field lines form a magnetic nozzle of sorts. The combination of the radial current and axial magnetic field produces an azimuthal force which causes the plasma to rotate, or swirl, around the central axis. The applied field also has the effect of creating a significant azimuthal, or Hall component to the discharge current. Four main acceleration mechanisms are produced:

- The Hall acceleration, due to the Lorentz force produced by the interaction of the Hall current and the applied field.
- The self-field acceleration, due to the interaction of the radial discharge current and the self-induced magnetic field.
- The swirl acceleration, which is caused as a byproduct of the swirling motion of the plasma and the subsequent expansion in the magnetic nozzle.
- The gas-dynamic, or thermal acceleration, caused due to the thermodynamic expansion of the hot gases in the thruster.

The operating principle of AF-MPDT is shown in Figure 4.

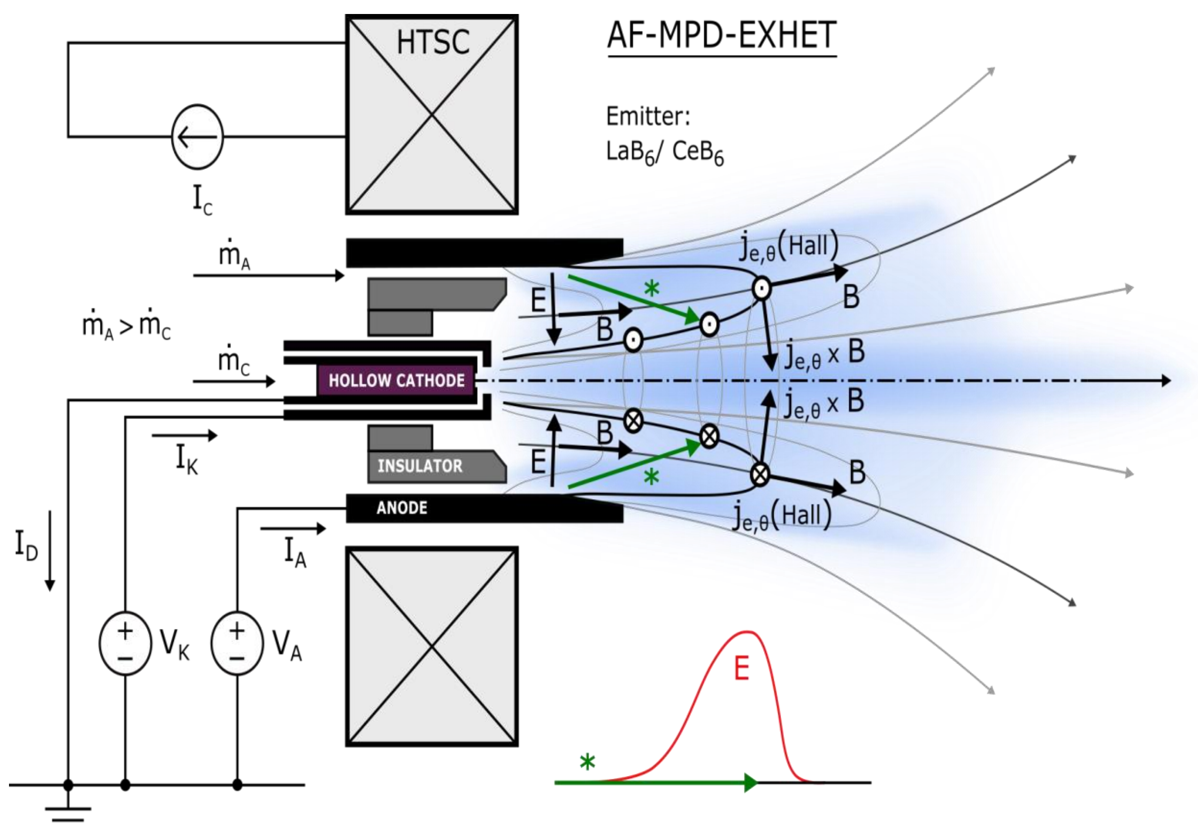

Figure 4. Operating Principle of AF-MPDT[11]

The self-field acceleration is dependent only on the discharge current, *j*, and scales quadratically with the current. The Hall and swirl accelerations are not found in self-field designs. These scale linearly with both *j* and the applied magnetic field *B*. Due to the high currents required to produce a significant self-field acceleration, the Hall and swirl accelerations are generally the most relevant for AF-MPDT. To maintain the performance of these acceleration mechanisms at lower discharge currents, higher magnetic field strengths are required. The use of HTS allows the generation of much stronger magnetic fields, thus enabling operation at lower discharge currents and higher voltages, which in turn positively impacts the thruster lifetime.

The system architecture presented in this section is based on the SX3 thruster[15]: a 100kW AF-MPDT prototype developed and characterised at the University of Stuttgart, which uses copper electromagnets to generate the applied field. In this context, HTS coils replace these magnets. This technology iserein referred to as SUPREME (SUPerconductor-based Readiness Enhanced Magnetoplasmadynamic Electric Propulsion).

The SUPREME concept consists of six subsystems:

- The applied-field (AF) module, consisting of the HTS coils and the cryogenic system.
- The discharge unit, consisting of the anode, cathode, thermal & electric insulators, and the propellant injection system.
- The power processing unit (PPU), controlling the cathode heater, keeper, and discharge.
- The thermal management sub-system, including passive components such as multi-layer insulation and radiators.
- The propellant supply system, including the propellant storage, pressure regulators, and flow control system.
- The spacecraft interfaces, which integrate the EPS with the spacecraft electrical and mechanical interfaces.

These subsystems are shown in a conceptual design in Figure 5. The incorporation of HTS coils has the greatest impact on the discharge unit and the applied-field module. As such, these will be the focus of this section.

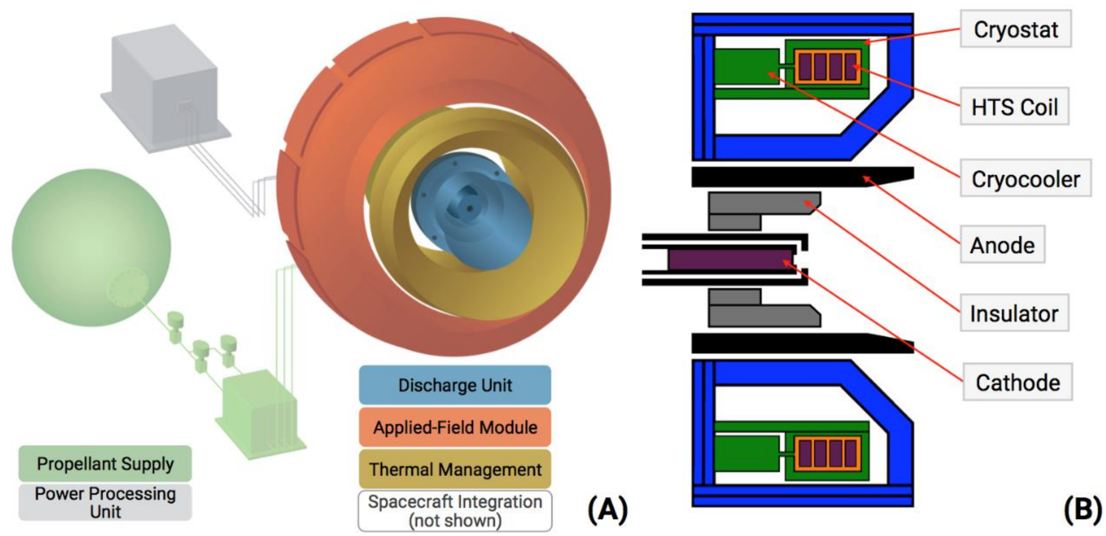

Figure 5. Conceptual design of the SUPREME Thruster (A) Subsystem Breakdown (B) Cross-sectional View

A. Applied-Field Module

HTS coils generate magnetic fields in the same way as the electromagnets they replace through electromagnetic phenomena. The coils are positioned concentric with the thruster anode and cathode. HTS provide operational flexibility and can be scaled up with the thruster, only suffering extremely small mass and volume penalties. The HTS coils have a current density of 100-500 A/mm^2 [16]. The exact critical current is dependent on the strength of the magnetic field and on any external perturbations such as the electromagnetic characteristics of the discharge.

The operation of AF-MPDTs at discharge currents as low as a few hundred Amps requires the generation of magnetic fields above 1T[2]. With these high current densities, the HTS coils can generate these magnetic fields with relatively low power consumption while allowing for efficient thruster operation at higher voltages and low discharge currents. As such, the HTS tape used to produce the coils is only 12mm wide and 100µm thick. By adjusting the coil input current, the strength and shape of the magnetic field is altered, thus enabling throttling of the thruster over a wide operational range.

The primary challenge for the HTS coils is the need to maintain them at a temperature below their critical temperature. Above this temperature, the coils experience a sudden gain in resistance. If this temperature is exceeded during operation, the HTS coils are "quenched" i.e. the resistance increases sharply. This phenomenon can result in significant damage to the superconductors. Thus, the maintenance of the HTS temperature is of significant importance. A cryogenic cooling system is thus included in the system architecture as part of the AF-module. The HTS tapes are embedded within a cryostat, which is maintained below the critical temperature by the cryocooler. Cryogenic cooling systems are an industrially mature technology with existing spaceflight heritage.[17, 18] The cryogenic cooling system uses a reverse Turbo-Brayton cycle and neon as the working fluid, with closed-loop operational temperatures between 30 and 80 K. The use of helium or nitrogen is also a possibility, depending on the HTS material.

The cryogenic system is compact and requires a relatively small amount of power. For a 20kW thruster, the applied-field module has a power consumption around 5% of the total thruster input power. A conceptual HTS coil for use in a 20kW SUPREME thruster is displayed in Figure 6.

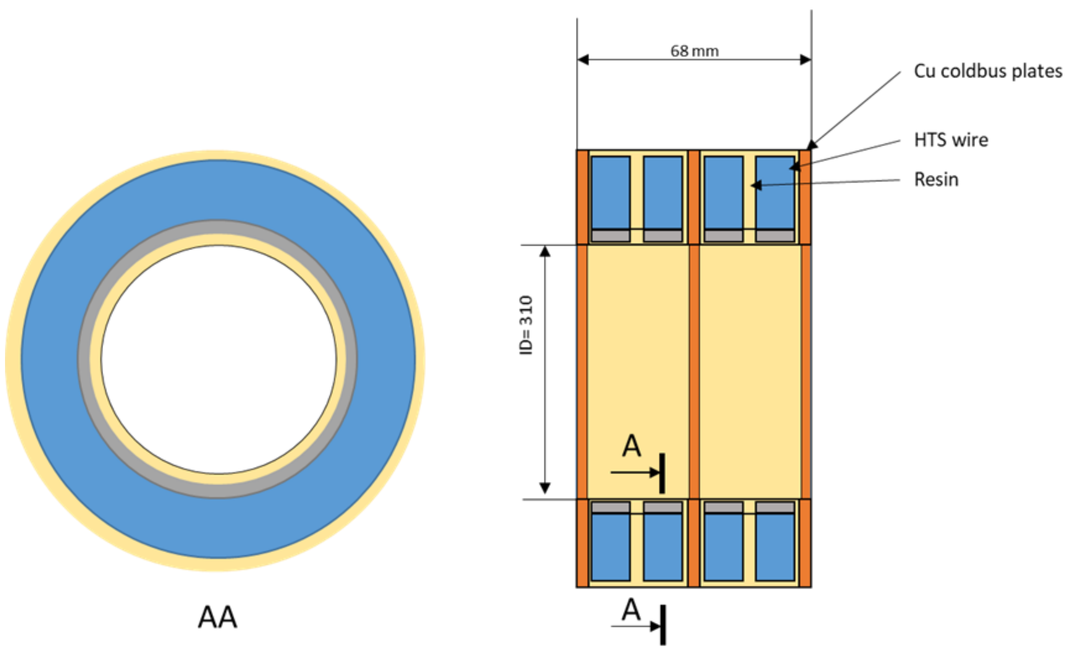

Figure 6. Conceptual design for 20kW Applied-Field Module incorporating HTS Coils

The HTS coil for the 20kW SUPREME thruster design will have an inner diameter of about 31cm and will be capable of generating a magnetic field strength of at least 0.8T. Operational magnetic field strengths of up to 1.5T are expected. The overall applied-field module including both the HTS coil and the cryogenic system will weigh approximately 35kg, and the discharge unit will weigh approximately 10kg, giving an overall thruster mass of 45kg. For the 100kW design, these numbers are expected to rise to 45kg, 25kg and 70kg respectively. The specific weight of the design is thus 2.25 kg/kW for the 20kW model, add 0.7 kg/kW for the 100kW model, indicating the excellent scaling potential of the technology.

A further application of HTS would be in a magnetic thrust-vector control (TVC) system. For current EPS, TVC can only be achieved by mounting the thrusters on mechanical gimbals which orientate the thruster as needed. These gimbals are typically 50% of the overall thruster mass,[19] and are a single point of failure for thruster orientation. In the SUPREME architecture, the inclusion of a separate HTS unit in the AF-module, positioned downstream of the main acceleration coil towards the thruster exhaust, can act as a magnetic TVC system. By using a helix saddle coil geometry, a tailored magnetic field can be created to deflect the accelerated ions and thus re-orientate the thruster exhaust plume. The direction of deflection can be altered by simply adjusting the current through the coils, with no moving parts. Such a system would significantly reduce the thruster system mass, and remove potential point of mechanical failure.

B. Discharge Unit

The discharge unit consists primarily of the anode, cathode, and propellant injection system. These are positioned concentrically within the HTS coils and the AF-module. This simple coaxial configuration is advantageous for the design, manufacturing and assembly of the thruster, as well as for scaling up the technology to higher powers. Under the SUPREME approach two main modes of operation are conceived depending on the operational voltage: either voltage regulated operation at 300 – 750 V, or direct drive operation up to 300 V. While direct drive operation will allow the usage of a simpler and higher efficiency PPU, voltage regulation benefits from the technology transfer of PPU's from existing HET systems. Both modes of operation can be used in a wide range of powers surpassing the operational capabilities of other high-power EP technologies.

1. Anode

The anode is the outer of the two electrodes and acts as the positive terminal of the discharge unit. The anode is a source of losses due to anode heating, thus resulting in lower thrust efficiencies. This heating can be attributed to the anode fall voltage, a phenomenon that occurs due to the formation of an un-ionised sheath at the anode. This un-ionised boundary layer has a high electric resistance, causing a fraction of the electrical potential between the electrodes to be wasted as heat and resulting in an effective voltage drop. The anode fall voltage is the voltage corresponding to the power loss which occurs between the edge of the sheath and the anode; thus, a lower fall voltage is desirable as this indicates a lower power loss and thus fewer losses in the sheath. The anode design must therefore focus on minimizing the fall voltage. This can be achieved by using a material with a moderate work function, which reduces electron emission and thus reduces the fall voltage. Furthermore, customised gas channels can be incorporated in the anode to inject gas at the points where arc attachment occurs, further nullifying the impact of the anode fall voltage.

2. Cathode

The cathode is located on the central axis of the thruster. The cathode is prone to erosion due to the high currents present in AF-MPDTs, and thus is one of the components which limits the lifetime of current designs. The introduction of HTS coils into the system architecture allows thruster performance to be maintained at a lower discharge current (<180A). Operating at low discharge currents enables the use of hollow cathode technology and hence significantly longer cathode lifetimes. This reduces the effect of electrode erosion on the cathode, thus increasing the lifetime of the component and overcoming one of the fundamental obstacles facing a flight-ready AF-MPDT. The lower discharge current also facilitates the use of other materials in the cathode. For example, LaB6 inserts can be used as thermionic emitters instead of thoriated tungsten bulk cathodes resulting in increased operational stability over a wider operational regime. The former is known to be more stable during operation and are more robust and flexible at ignition conditions.[20]

C. Other subsystems

3. Power processing

The PPU combines three different technologies, i.e. the PPU modules that supply and control the discharge unit, supply and control the cryogenic system and supply and control the HTS coils. The operational voltage characteristics of the SUPREME laboratory prototype will resemble those of HET. Thus, there is an expected benefit from this heritage in the approach and adaptation of a PPU design for an AF-MPDT discharge module. The two latter modules will for the first time be adapted to a thruster technology. For power classes higher than 250 kW operated in direct drive mode, the design requirements of the PPU are reduced.

Especially at these higher power classes, the inclusion of HTS can impact spacecraft design beyond the EPS itself. The most promising application is for high-power transmission lines, which can be replaced by superconducting DC bus bars, drastically reducing the mass and volume of these components.[16]

D. Thruster Characteristics

The introduction of HTS increases the operational range of the thruster due to the increased range of magnetic field strengths which can be generated. This allows throttleability of the SUPREME thruster, providing the capability to operate over a wide range of specific impulses. As such, a single thruster design can be utilised for a variety of different missions just by altering the operational mode. This is a core competitive advantage of the SUPREME design over other technologies, which would require different optimised designs in order to operate at the optimum I_{sp} level of a particular mission. This translates into an economical advantage whereby the same thruster design can take advantage of economies of scale by maintaining a single manufacturing assembly line regardless of the specific mission application. The predicted operational range of the thruster is shown in Figure 7.

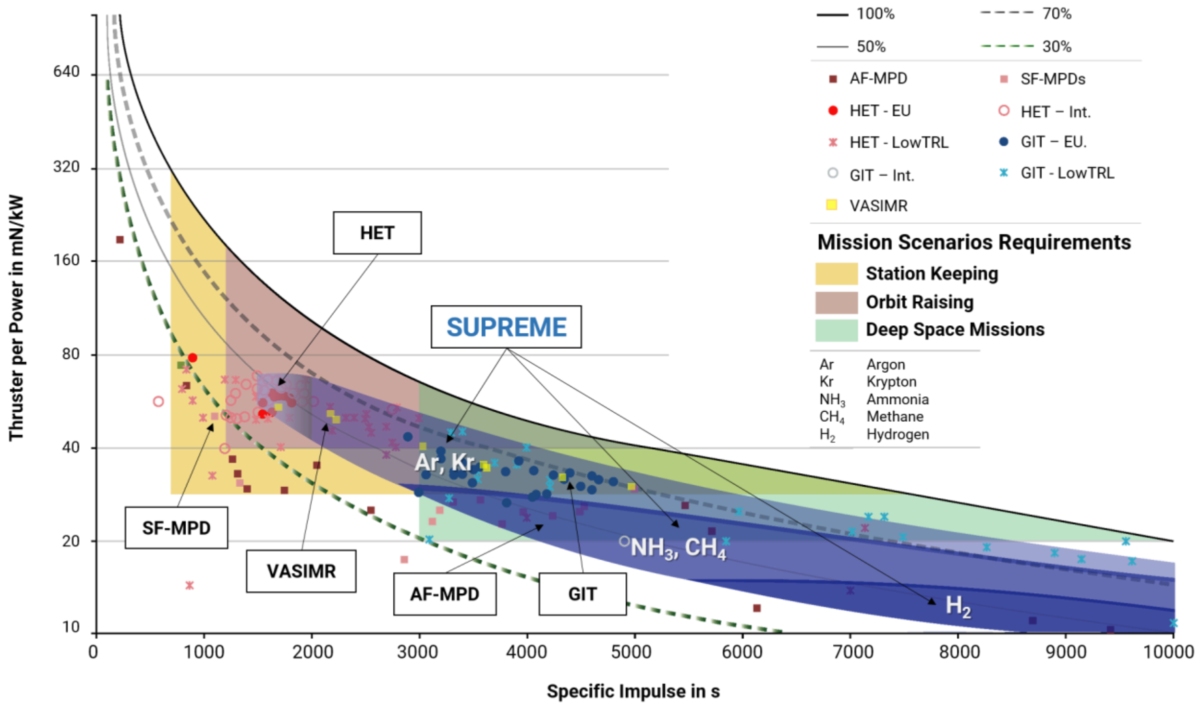

Figure 7. Predicted operating range of the SUPREME thruster[21]

V. Market analysis and mission scenarios for Applied-Field Magnetoplasmadynamic Thrusters

AF-MPDTs are suitable for a variety of space mission applications. However, their primary value proposition is best applied to high ΔV scenarios where fast transfers of heavy cargo with a suitable exhaust velocity are required. While the current market popularity is focused on small satellites and constellations, there is also a growing interest in higher power missions, evidenced by the opening of contracts for the ESA Mars Sample Return mission[22] (42kW) and the award of the contract for the Lunar Orbital Gateway Power & Propulsion Element[23] (50kW). Furthermore, several funded studies have explored the architectures of lunar and Mars cargo missions, and high-power GEO communications satellites remain a cornerstone of the commercial market. An interesting development in the coming years will be the introduction of space tugs to the market, as evidenced by the appearance of several start-ups in this sector. These spacecraft will have multi-use applications in areas such as orbit-raising (MOMENTUS Space, ATOMOS Nuclear & Space), refuelling (OrbitFab), satellite servicing (Effective Space) and debris removal/management (e.Deorbit).

With this in mind, the following sections consider three mission scenarios. From a mid-term market perspective, orbit-raising of GEO satellites using a space tug is presented. From a long-term perspective, the study focuses on cargo missions to the Moon and lastly to Mars. For each mission scenario, a reference architecture is identified from literature which is used as the baseline for our cost analysis.

E. Orbit raising for GEO satellites

Orbit raising of large satellites to GEO is one of the mission scenarios for which space tugs are conceived and where the SUPREME 20kW could gain full flight heritage. The market share for GEO satellites is 5.9% for satellites below 1.5 tonnes, 34.4% for satellites weighing between 1.5 and 3.5 tonnes, 39.9% between 3.5 and 5.5 tonnes, and

19.8% for those above 5.5 tonnes[24]. The latter have thus far been the largest GEO satellites and the principal target for SUPREME technology. Considering that the market volume for orbit raising of GEO satellites above 1 tonne is about 10 missions per year, there are at least 2 missions per year that a space tug equipped with SUPREME can perform.

The required ΔV of about 2387 m/s to reach GEO from a GTO injection orbit is a motivating factor for efficient EPS to increase propellant mass savings. Such transfers typically have a 6-month maximum time constraint for commercial reasons. In this sense, the correct operational regime must be selected to ensure a sufficiently high thrust to achieve this target duration. Furthermore, the space tug mission architecture makes use of several repeated trips between LEO and GEO, thus increasing the total mission ΔV severalfold. Orbit-raising space tug missions can vary greatly depending on the mass of the tug, the input power, the number of trips, and the mass of the satellite to be transported. Several studies[25, 26] have already been performed on this topic with a wide variety of these parameters. For simplicity, and to maintain consistent methodology with the other missions, only a single transfer is considered in the calculations for this mission, using a 40kW space tug utilising two SUPREME thrusters. This corresponds to two 20kW HT20k thrusters, or eight 5kW T6 thrusters. A 6500kg satellite is considered as the payload.

F. Lunar Cargo Missions

Lunar missions have seen a great deal of interest in recent years, with the progression of the Lunar Gateway mission and the formation of several Moon-related start-ups (Astrobotic, Space Mining Technologies, etc.). Furthermore, the establishment of human presence on the surface of the moon is a clear objective for several national space agencies. Both this and in-space bases such as the Lunar Gateway will require regular cargo replenishment to sustain operation activities. Cargo masses greater than approximately 8 tonnes are beyond the trans-lunar injection capabilities of current launch vehicles.[27] Any larger payloads will require transportation from LEO to the moon.

The lunar mission architecture proposed by Spores[28], starting from LEO, requires a ΔV around 7800 m/s to deliver 27 tonnes of cargo to Low Lunar Orbit. Two power classes are considered: a 160kW mission, and a 600kW mission. The 160kW mission considers a cluster of 8 20kW SUPREME thrusters compared with a similar cluster of HT20k HET thrusters. While a cluster of 4 40kW thrusters would be a more optimum solution, a system of this power class is not considered in the SUPREME commercialisation plan. T6 GITs are not considered here due to the unrealistic clustering of 32 units required. The 600kW mission considers a cluster of 6 100kW SUPEME thrusters compared with the same configuration of HET X3 thrusters or 3 VASIMR systems.

G. Mars missions

As with the Moon, there are widespread ambitions in the space industry for human colonisation of Mars. Any such permanent human activity on Mars will require cargo resupplies. Considering the masses of cargo required and the transfer distance between Earth and Mars, no current launch vehicle is capable of providing a direct injection trajectory as in the case of the Moon. Thus, this mission will require transportation from LEO to Mars orbit.

The Mars mission architecture proposed by Gilland[29], starting from LEO, requires a ΔV in the order of 13500 m/s. This can vary depending on the thrust level and the mission scenario. This mission considers an input power of 1MW, corresponding to a cluster of 10 100kW SUPREME thrusters. This is compared with a cluster of 10 HET X3 thrusters or 5 VASIMR systems.

H. Analysis

For all the mission scenarios, the same analysis approach is used. Mission parameters, such as delta V, spacecraft and cargo mass, and available input power are taken from reference mission architectures found in existing literature. The characteristics of an AF-MPDT EPS are then substituted into these reference missions and the effects on the mission masses are evaluated. A simplified mission architecture in which a "transportation" spacecraft delivers a cargo mass to its destination before returning to the starting point is used as a basis for calculations. Detailed mission analysis is beyond the scope of this study, and thus the difference in delta V due to alternate trajectories is assumed to be insignificant.

The same calculations are performed using estimated performance and mass characteristics of competing EP technologies. Missions using the 20kW SUPREME system are compared with HT20k HET from SITAEL and the T6 GIT from QinetiQ. Missions using the 100kW SUPREME system are compared with the X3 Nested HET from Aerojet Rocketdyne, and VASIMR from Ad Astra Rocket. Primarily, the EPS mass and propellant mass of the spacecraft are affected. The cost savings for each mission are evaluated based on the difference in launch costs and propellant costs. The launch costs are evaluated based on the total spacecraft mass to be launched and using a standard 'per kg' launch price.

The methodology of this study is presented in this section. The methodology considers two dry masses: the mass of the transfer vehicle and the mass of the cargo vehicle. The transfer vehicle consists of the EPS, propellant tanks, and any other supporting equipment such as attitude control, communications, structure, robotics and thermal management systems. The propellant tank mass is calculated assuming a spherical tank made of titanium with a wall thickness of 2mm. The remaining mass of the transfer vehicle and the cargo vehicle mass are taken directly from the reference mission.

The following parameters are taken as inputs to the calculation procedure:

- Specific Impulse I_{sp} (s)
- Thruster Power P_{in} (kW)
- Thrust Efficiency η
- Thruster Specific Weight γ_t (kg/kW)
- PPU Specific Weight γ_p (kg/kW)

The thrust density is calculated from these parameters as follows:

$$Thrust\ Density\ \alpha = \frac{2\eta}{I_{sp} g_0} \quad (1)$$

In this case, the thruster specific weight consists of all thruster systems except the PPU and propellant tanks. The key parameters for each of the considered EPS are displayed in Table 1.

Table 1. Key EPS parameters for each technology considered

	LOW POWER		
Parameter	**GIT (QinetiQ T6)**[30,31]	**HET (SITAEL HT20k) *** [32]	**SUPREME 20kW**
Specific Impulse (s)	4120	2520	4000
Thruster Input Power (kW)	5	20	20
Thrust Efficiency	0.636	0.63	0.65
Thrust Density (mN/kW)	31.17	50.97	30.58
Thruster Specific Weight (kg/kW)	2.49	2.5	2.25
PPU Specific Weight[33]	10	5	5
Propellant	Xenon	Xenon	Argon
	HIGH POWER		
	HET (X3)[34]	**VASIMR**** [35]	**SUPREME 100kW**
Specific Impulse (s)	2600	5000	5000
Thruster Input Power (kW)	100	200	100
Thrust Efficiency	0.67	0.6	0.75
Thrust Density (mN/kW)	52.54	24.46	30.58
Thruster Specific Weight (kg/kW)	2.3	10	0.7
PPU Specific Weight[33]	5	n/a	5
Propellant	Xenon	Argon	Argon

* The mass of the HT20k system is estimated based on a typical HET specific weight
**The mass of the VASIMR system is estimated as an overall system mass with PPUs included.

Mission parameters required for the mission analysis are:

- Cargo Vehicle Mass m_{cargo} (kg)
- Transfer Vehicle Mass m_{tv} (kg)
- Total Mission Power P_{tot} (kW)
- ΔV_{out} (Outbound) (m/s)
- ΔV_{in} (Inbound) (m/s)

The parameters for each mission under consideration are shown in Table 2.

Table 2. Mission parameters for each assessed mission

Mission Parameter	Orbit Raising 40kW	Lunar Cargo 160kW	Lunar Cargo 600kW	Mars Cargo 1MW
Transfer Vehicle Dry Mass excl. propulsion system (kg)	675*	2700	6800	22950
Delivered cargo mass (kg)	6500	27000	27000	100000
Mission Power (kW)	40	160	600	1000
Outbound ΔV (m/s)	2387.7	7830	7830	13500
Inbound ΔV (m/s)	2387.7	7840	7840	n/a

*The space tug dry mass is assumed as 25% of the tug in the 160kW case

For each mission and EPS the following can be calculated:

$$EPS\ Mass\ m_{eps} = (\gamma_t + \gamma_p) * P_{tot} \qquad (2)$$

The calculation is bounded by the final mass of the mission, i.e. when the transfer vehicle has returned to LEO for refuelling. This final mass is thus the transfer vehicle dry mass. This is calculated using the numbers from Table 2, to which the EPS system mass as calculated by Eq. 3 is added. Unlike the other contributions to the transfer vehicle mass, the tank mass is dependent on the amount of propellant required as well as its storage density, thus this must be iterated to reach a final value. The first iteration therefore ignores the tank mass.

Next, the mass of the transfer vehicle when leaving the Moon is calculated. At this point this is equal to the dry mass and the mass of the propellant required for the journey. This can be calculated using the basic form of the rocket equation.

$$Mass\ at\ Moon\ departure\ m_{md} = \exp\left(\frac{\Delta V_{in}}{I_{sp} g_0}\right) *\ m_{tv} \qquad (3)$$

From this, the mass of the spacecraft can be calculated when arriving at the Moon by adding the mass of the cargo vehicle.

$$Mass\ at\ Moon\ arrival\ m_{ma} = m_{md} + m_{cargo} \qquad (4)$$

The starting mass of the spacecraft in LEO can be calculated by again using the rocket equation.

$$Mass\ at\ Earth\ departure\ m_{ed} = \exp\left(\frac{\Delta V_{out}}{I_{sp} g_0}\right) *\ m_{ma} \qquad (5)$$

The first iteration of these calculations will provide outbound and inbound propellant masses for the mission, giving a total mission propellant mass m_{prop}. These can be used to calculate the tank mass.

$$Propellant\ Tank\ Mass = \frac{4\pi\rho_{titanium}}{3}\left[\left(\left(\frac{3m_{prop}}{4\pi\rho_{prop}}\right)^{\frac{1}{3}} + 0.002\right)^3 - \frac{3m_{prop}}{4\pi\rho_{prop}}\right] \qquad (6)$$

The dry transfer vehicle mass is updated with the new tank mass and the calculation is iterated until convergence. In the case of the Mars cargo mission, where the transfer vehicle is assumed to remain at Mars after delivery, the calculation is simplified to a one-leg journey.

The calculation procedure returns values of propellant mass and spacecraft starting mass, and these can be used to calculate the cost savings. The propellant cost savings are calculated based on the unit price of the corresponding propellants (taken from a gas supplier), while the launch cost savings are calculated based on unit launch price per kg, as in Eq. 8 and Eq. 9. The propellant and launch costs, assuming a Falcon 9, are shown in Table 3.

Table 3. Launch and propellant costs

	Orbit Raising
Cost of Xenon (€/kg)	1500
Cost of Argon (€/kg)	7.50
Falcon 9 launch cost to LEO (€/kg)[36]	3690.18

$$Propellant\ Cost\ Savings = (m_{xe} * \$_{xe}) - (m_{ar} * \$_{ar}) \quad (8)$$

$$Launch\ Cost\ Savings = (m_{comp} - m_{\text{sup}}) * \$_{kg} \quad (9)$$

For comparison purposes, the firing time of each scenario is also calculated assuming a constant firing throughout the duration of the transfer from Eq. 10.

$$Firing\ Time\ \tau = \frac{m_{prop} I_{sp} g_0}{T} \quad (10)$$

The values and parameters calculated using this methodology are displayed for X3 and SUPREME for the 600kW Lunar Mission, in Table 4.

Table 4. Values from the calculation of the 600kW Mission, comparing SUPREME and X3

EP Parameters	SUPREME	HET X3
I_{sp} (s)	5000.00	2600.00
Power In (kW)	100.00	100.00
Efficiency	0.75	0.67
Thrust Density (mN/kW)	30.58	52.54
# Of Engines	6.00	6.00
Thrust (N)	18.35	31.52
Total Power In (kW)	600.00	600.00
Thruster specific weight (kg/kW)	0.70	2.30
PPU specific weight (kg/kW)	5.00	5.00
Mission Parameters		
Cargo Vehicle Mass (kg)	27000.00	27000.00
EPS Mass (kg)	3420.00	4380.00
Tank Mass (kg)	144.23	248.46
Transfer Vehicle Dry Mass (kg)	10364.23	11428.46
Return Leg		
Final Mass arriving back to Earth (kg)	10364.23	11428.46
Total Delta V Required (m/s)	7830	7840
Satellite Mass leaving moon (kg)	12160.55	15541.05
Propellant required (kg)	1796.32	4112.60
Firing Duration (days)	55.58	38.52
Outbound Leg		
Final Mass arriving to Moon (kg)	39160.55	42541.05
Total Delta V Required (GTO) (m/s)	7830	7830
Propellant required (kg)	6777.92	15285.97
Firing Duration (days)	209.71	143.16
Launch Mass of mission (kg)	45938.47	57827.02
Cost Calculations		
Launch Cost (€)	€169,521,165.09	€213,392,042.36
Propellant Cost (€)	€64,306.82	€29,097,847.87
Mission Cost (€)	€169,585,471.91	€242,489,890.24

VI. Discussion

The potential cost savings of using SUPREME systems are presented in the tables below. Table 5***Table 6*** shows the estimated mission cost for each mission using each EPS. Table 6 shows the maximum and minimum savings between these costs on a per-mission basis. Savings are captured due to cheaper propellant costs, and cheaper launch costs. Compared to GIT and HET systems, the propellant cost savings are high due to the high cost per kilogram of xenon compared with argon. Launch costs in these cases are also significantly higher for HET due to the reduced specific impulse of the system. The savings compared to VASIMR are smaller, as VASIMR can also operate with argon and can match the specific impulse of SUPREME. However, the SUPREME system masses are significantly lighter than VASIMR which contributes the majority of the savings. As expected, the mission savings are greatly increased as the power increases, indicating that high-power missions are the best application for SUPREME

Table 5. Launch and Propellant costs for each mission and EPS considered

	HT20k	**T6**	**SUPREME 20kW**
Orbit Raising Space-Tug	€32.2m	€31.1m	€29.6
Lunar Cargo 160kW	€185.6m	n/a	€143.6m
	X3	**VASIMR**	**SUPREME 100kW**
Lunar Cargo 600kW	€213.4m	€182.7m	€169.6m
Mars Cargo 1MW	€946.7m	€641.9m	€627.4m

Table 6. Total maximum and minimum mission savings for each mission scenario

	Maximum	Minimum
Orbit Raising Space-Tug	€2.6m	€1.5m
Lunar Cargo 160kW	€42.0m	€42.0m
Lunar Cargo 600kW	€43.8m	€13.1m
Mars Cargo 1MW	€319.3m	€14.5m

technology.

On the other hand, the savings for the orbit raising space tug are much smaller. This can be attributed to the lower ΔV and spacecraft masses of these missions, as well as the fact that only a single satellite transfer is considered. A commercially operating space tug will perform several transfers between re-fuelling; thus, the expected savings would be higher.

Figure 8 compare the propellant mass fraction and transfer times for the various EPS and missions. SUPREME consistently offers the lower propellant mass fraction, corresponding to lower launch costs. Although HET offers faster transfer times than SUPREME at the selected mission conditions, SUPREME outperforms VASIMR on this metric due to its higher thrust efficiencies.

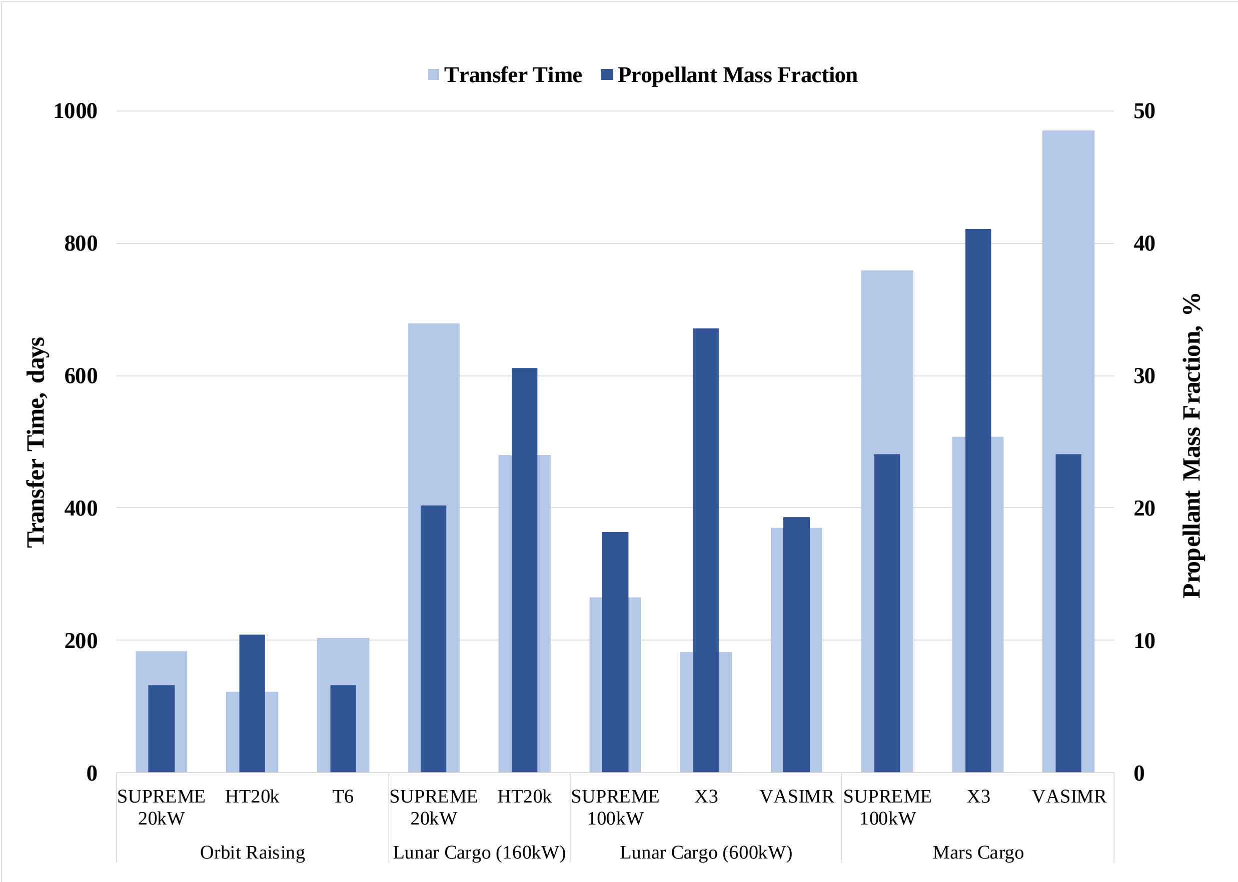

Figure 8. Comparison of transfer times and propellant mass fractions for the different EPS and mission scenarios.

VII. Conclusion

This paper has explored the potential of incorporating High-temperature Superconductors within Applied-Field Magnetoplasmadynamic thrusters. This key enabling technology leverages a significant research history to offer a system architecture which is simple and robust, and which can overcome the existing barriers to commercialisation such as lifetime and mass issues. Considering both this strong research heritage and its inherent suitability for high powers, AF-MPDTs are, from an economic and technological point of view, the strongest candidate for producing a marketable thruster to power the development of logistic operations in near-Earth orbit, interplanetary cargo missions as well as, the building of large space infrastructures. Existing technologies such as GIT and HET are highly suitable for the current mission power classes but face significant mass penalties when upscaling to higher unit powers. On the other hand, clustering becomes unfeasibly complicated and inefficient beyond a certain number of units. The use of xenon, an expensive and increasingly rare propellant, further impacts the economic considerations of high power missions. Thus, the usage of these technologies in higher power missions (>40kW) leads to unreasonable system masses and necessitates a more inherently scalable technology, which can operate with alternative propellants, in order to keep missions economically and technologically feasible.

While other technologies focused on high-power operation such as VASIMR are under development, the simplicity, scalability, robustness and research heritage of AF-MPDT positions SUPREME as the clear economical and technical choice for high-power missions. The analysis performed in this paper indicates that the replacement of these technologies with compact and efficient SUPREME technology will save several millions of Euros in mission costs. These savings can be attributed to two main factors: reduced spacecraft mass and therefore launch costs and reduced propellant costs. This is achieved by the lower power specific mass and higher I_{sp} of the SUPREME EPS, which requires less propellant for transfers and reduces the overall spacecraft mass, thus reducing launch costs. Meanwhile, the use of cheap and widely-available argon as a propellant ensures significant costs savings against xenon-fed systems. The analysis further indicates that the extent of these savings increases as the mission power increases, demonstrating the superiority of the technology for high-power operation.

References

[1] Herman, D. A. et al., "Overview of the Development and Mission Application of the Advanced Electric Propulsion System (AEPS)," *35th International Electric Propulsion Conference,* Atlanta, 2017.

[2] National Aeronautics and Space Administration, "NASA Technology Roadmaps. TA2: In-Space Propulsion Technologies," 2015.

[3] Hall, S. J. et al., "Implementation and Initial Validation of a 100-kW Class Nested-Channel Hall Thruster," *50th AIAA/ASME/SAE/ASEE Joint Propulsion Conference, AIAA Propulsion and Energy Forum,* Cleveland, 2014.

[4] Andrenucci, M., Biagioni, L., Marcuccio, S., and Paganucci, F., "Fundamental Scaling Laws for Electric Propulsion Concepts. Part 1: Hall Effect Thrusters," *28th International Electric Propulsion Conference*¸ Toulouse, 2003.

[5] Nerheim, N. M., and Kelly, A. J., "A Critical Review of the State-of-the-Art MPD Thruster," *AIAA Electric Propulsion and Plasmadynamics conference,* Colorado Springs, 1967.

[6] Andrenucci, M., "Magnetoplasmadynamic thrusters; Encyclopedia of Aerospace Engineering," DOI: 10.1002/9780470686652.eae118.

[7] Kruelle, G. and Zeyfang, E., "Preliminary Conclusions of Continuous Applied Field Electromagnetic Thruster Research at DFLVR," *11th International Electric Propulsion Conference,* New Orleans, 1975.

[8] Mantenieks, M. A. and Myers, R. M., "Preliminary Test Results of a Hollow Cathode MPD Thruster," *22nd International Electric Propulsion Conference*, Viareggio, 1991.

[9] Gorshkov, O. A., Shutov, V. N., Kozubsky, K. N., Ostrovsky, V. G., Obukhov, V. A., "Development of High Power Magnetoplasmadynamic Thrusters in the USSR," *30th International Electric Propulsion Conference*, Florence, 2007.

[10] Tahara, H. and Kagara, Y., "Performance and Plasma Characteristics of a Cusp and Divergent-Nozzle Applied-Magnetic-Field MPD Thruster," *30th International Electric Propulsion Conference,* Florence, 2007.

[11] Boxberger, A., and Herdrich, G., "Integral Measurements of 100 kW Class Steady State Applied-Field Magnetoplasmadynamic Thruster SX3 and Perspectives of AF-MPD Technology," *35th International Electric Propulsion Conference*, Atlanta, 2017.

[12] Kitaeva, A., Tang, H., Wang, B. and Andresussi, T., "Optimization of the AF-MPDT Geometry and Operating Parameters for the Low Current to Mass Flow Rate Regime," *Plasmadynamics and Lasers Conference*, Atlanta, 2018.

[13] Sasoh, A., Kasuga, H., Nakagawa, Y., Matsuba, T., Ichihara, D., and Iwakawa, A., "Electrostatic-Magnetic-Hybrid Thrust Generation in Central-Cathode Electrostatic Thruster (CC-EST)," *Acta Astronautica 152*, 2018.

[14] Lev, D. and Choueiri, E. Y., "Scaling of Anode Sheath Voltage Fall with the Operational Parameters in Applied-Field MPD Thrusters," *32nd International Electric Propulsion Conference,* Wiesbaden, 2011.

[15] Boxberger, A., and Herdrich, G., "Integral Measurements of 100 kW Class Steady State Applied-Field Magnetoplasmadynamic Thruster SX3 and Perspectives of AF-MPD Technology," *35th International Electric Propulsion Conference*, Atlanta, 2017.

[16] La Rosa Betancourt, M., Boxberger, A., Herdrich, G., Bauer, M., "High Temperature Superconductors as Game Changers for Plasma Based Space Propulsion Systems for GEO Satellites, Drag Compensation of Large Space Structures and Beyond Earth Orbit Missions," *Space Propulsion Conference,* Seville, 2018

[17] Tanchon, J., Lacapere, J., Rey, J., Molyneaux, A. and Paganucci, F., "A 40K Turbo-Brayton cryocooler for Earth Observation Applications," *20th International Cryocooler Conference,* Boulder, 2018

[18] Tanchon, J. et al., "A Turbo-Brayton Cryocooler for Future European Observation Satellite Generation, *19th International Cryocooler Conference,* San Diego, 2016.

[19] Hofer, R. R., Randolph, T. M., "Mass and Cost Model for Selecting Thruster Size in Electric Propulsion System," *Journal of Propulsion and Power,* Vol. 29, No. 1, 2013

[20] Fradkin, D. B., Blackstock, A. W., Roehling D. J., Stratton, T. F., Williams, M., and Liewer, K. W., "Experiments using a 25 kW hollow cathode lithium vapor MPD arcjet," *AIAA Journal,* Bd. 8, Nr. 5, pp. 886-894, 1970.

[21] Peuker, L. and Wollenhaupt, B., "OHB System's View on Electric Propulsion Needs," *Epic Workshop,* Brussels, 2014.

[22] Sutherland, O., "Mars Sample Return – Earth Return Orbiter," *ESA Industry Day Presentation,* 2019.

[23] NASA Awards Artemis Contract for Lunar Gateway Power, Propulsion, https://www.nasa.gov/press-release/nasa-awards-artemis-contract-for-lunar-gateway-power-propulsion [cited 14 September 2019].

[24] Union of Concerned Scientists, "UCS Satellite Database", USA, 2019.
[25] Mammarella, M., Paissoni, C. A., Fusaro, R., Viola, N., Andreussi, T., Rossodivita, A., "A 20kw-class Hall Effect Thruster to Enhance Present and Future Space Missions," *69th International Astronautical Congress*, Bremen, 2018.
[26] Aleina, S. C., Viola, N., Stesina, F., Viscio, M. A., Ferraris, S., "Reusable Space Tug Concept and Mission," *Acta Astronautica 128*, 2016.
[27] Ariane 6 User's Manual, Issue 1, Arianespace, 2018.
[28] Spores, R., et al., "A Solar Electric Propulsion Cargo Vehicle to Support NASA Lunar Exploration Program," *29th International Electric Propulsion Conference*, Princeton, 2005.
[29] Gilland, J. H., LaPointe, L. R., Oleson, S., Mercer, C., Pencil, E., Mason, L., "MW-Class Electric Propulsion System Designs for Mars Cargo Transport," *AIAA Space 2011 Conference & Exposition*, Long Beach, 2011.
[30] Snyder, J. S., Goebel, D. M., Hofer, R. R., Polk, J. E., Wallace, N. C., Simpson, H., "Performance Evaluation of the T6 Ion Engine," *46th AIAA/ASME/SAE/ASEE Joint Propulsion Conference & Exhibit*, Nashville, 2010.
[31] Hall, K., "QinetiQ Electric Propulsion Gridded Ion Thruster Developments," *Epic Workshop*, Madrid, 2017.
[32] Leporini, A., et al., "Development of a 20 kW-Class Hall Effect Thruster", *Space Propulsion Conference*, Rome, 2016.
[33] Gonzales Del Amo, J., Di Cara, D. M., "Electric Propulsion Technology Overview," 2019.
[34] Hall, J. S., et al., "Update on the Nested Hall Thruster Subsystem for the NextSTEP XR-100 Program," *Joint Propulsion Conference, AIAA Propulsion and Energy Forum*, Cincinnati, 2018.
[35] Bering, III, E. A., et al., "Performance Studies of the VASIMR VX-200," *49th AIAA Aerospace Sciences Meeting and Exhibit*, Orlando, 2011.
[36] Federal Aviation Administration, "The Annual Compendium of Commercial Space Transportation:2018".